2014 International Conference on Unmanned Aircraft Systems (ICUAS)
May 27-30, 2014. Orlando, FL, USA

Design of Robust Controller of Fixed-Wing UAV for Transition Flight

Satoshi Kohno
Department of Aerospace Engineering
Nihon University, Chiba 274-8501, Japan
tetsu_0901cst@yahoo.co.jp

Kenji Uchiyama
Department of Aerospace Engineering
Nihon University, Chiba 274-8501, Japan
uchiyama@aero.cst.nihon-u.ac.jp

***Abstract*— We propose the flight control system of a fixed-wing small UAV for a transition flight in consideration of nonlinearity on its dynamics. The control system consists of controllers for translational motion and rotational motion. The effect of its nonlinear dynamics on a control performance cannot be disregarded when designing a flight control system because it is difficult to linearize the motion with consideration of an equilibrium transition between vertical and horizontal flight modes. Moreover, the attitude of the small UAV is particularly affected by disturbances such as a gust of wind. Therefore, we employ the dynamic inversion method to take nonlinearity of the motion into account for a flight control design. A robust controller is applied to control the attitude of the UAV. It is necessary to use an observer based on the disturbance accommodating control (DAC) method to estimate of unknown parameter of nonlinear equations. We present preliminary results of numerical simulations and experiments of the UAV testbed that uses the proposed control system.**

Keywords—fixed-wing UAV; transition flight; dynamic inversion method; DAC observer

I. INTRODUCTION

Unmanned Aerial Vehicle (UAV) has been actively developed all over the world since UAVs can accomplish dangerous missions such as disaster monitoring and atmospheric observation. An aircraft can be roughly classified into two types: a fixed-wing and a rotary-wing. A fixed-wing UAV can perform with higher speed and lower fuel consumption than a rotary-wing UAV. The UAV is appropriate for a fixed-point observation in monitoring a disaster area because of hovering capability. On the other hand, tilt-wing UAVs, which possess advantages of a fixed-wing and a rotary-wing UAVs, have become of interest lately[1],[2]. However, it is difficult to design a flight control system due to those complicated structure and nonlinear dynamics. It is especially important to discuss a transition flight of the UAV between a level flight to hovering. Myrand-Lapierre[3] et al. achieved experimentally the transition flight by switching the level flight controller and the hovering controller. A problem seems to lie in the controller that the control system did not consider the stability of the flight control system during transition.

We propose the flight control system without switching controller gains and dynamical model. Quaternion is used for the attitude angle expression of fixed-wing UAV instead of Euler angle. Nonlinear equations of motion are linearized by the dynamic inversion method[4]. A robust controller is applied to the linearized system, and to suppress the influence of disturbance such as wind. An observer based on the disturbance accommodating control (DAC) method[5] and the extended Kalman filter[6] are employed to estimate nonlinear terms with respect to aerodynamic forces and state variables of the UAV, respectively. We verify the validity of proposed flight control system through numerical simulations and experiments.

II. DYNAMICS

A. Parameter definitions

State variables and control inputs of a UAV are defined as shown Fig.1. An inertial coordinate system is fixed by earth's surface. The origin of the body-fixed coordinate system coincides with the center of mass of the UAV.

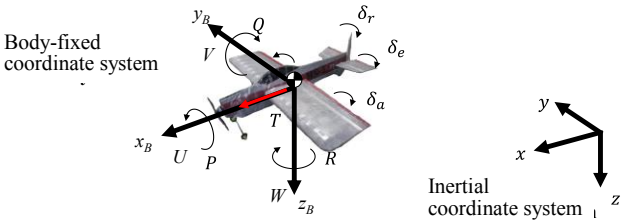

Fig. 1. Coordinate systems and parameter definitions.

U, V, and W represent velocities of UAV along x_B, y_B, and z_B axes, respectively. P, Q, and R denote the angular velocities around each axis. The attitude of UAV is controlled by regulating deflections of the aileron δ_a, the elevator δ_e and rudder δ_r. In addition, the thrust T that is generated by the nose mounted-propeller is also treated as a control input.

B. Equations of Motion

The nonlinear equations of motion are expressed as translational and rotational motion.

$$\dot{\mathbf{V}} = -\tilde{\boldsymbol{\omega}}\mathbf{V} + \mathbf{C}^{B/I}\mathbf{g} + \{\mathbf{C}(\alpha)\mathbf{F} + \mathbf{T}\}/m \quad (1)$$

$$\dot{\boldsymbol{\omega}} = -\mathbf{J}^{-1}\tilde{\boldsymbol{\omega}}\mathbf{J}\boldsymbol{\omega} + \mathbf{J}^{-1}\mathbf{M} + \mathbf{J}^{-1}\mathbf{M}_u\mathbf{u} \quad (2)$$

where

$$\mathbf{V} = [U \quad V \quad W]^T, \boldsymbol{\omega} = [P \quad Q \quad R]^T, \mathbf{g} = [0 \quad 0 \quad g]^T$$
$$\mathbf{T} = [T \quad 0 \quad 0]^T, , \mathbf{u} = [\delta_a \quad \delta_e \quad \delta_r]^T$$

$$\tilde{\boldsymbol{\omega}} = \begin{bmatrix} 0 & -R & Q \\ R & 0 & -P \\ -Q & P & 0 \end{bmatrix}, \mathbf{F} = \bar{q}S \begin{bmatrix} -C_D(\alpha) \\ C_y(\beta) + C_{yR}R + C_{y\delta_r}\delta_r \\ C_L(\alpha) + C_{L\delta_e}\delta_e \end{bmatrix}$$

$$\mathbf{C}(\alpha) = \begin{bmatrix} \cos(\alpha) & 0 & -\sin(\alpha) \\ 0 & 1 & 0 \\ \sin(\alpha) & 0 & \cos(\alpha) \end{bmatrix}, \mathbf{J} = \begin{bmatrix} I_{xx} & 0 & -I_{xz} \\ 0 & I_{yy} & 0 \\ -I_{xz} & 0 & I_{zz} \end{bmatrix}$$

$$\mathbf{M} = \bar{q}S \begin{bmatrix} b\{C_l(\beta) + C_{lP}P + C_{lR}R\} \\ c\{C_m(\alpha) + C_m(\dot{\alpha}) + C_{m_Q}Q \\ b\{C_n(\beta) + C_{nP}P + C_{nR}R\} \end{bmatrix} + \begin{bmatrix} -M_{drag} - I_{prop}\dot{\omega}_{prop} \\ -I_{prop}\omega_{prop}R \\ I_{prop}\omega_{prop}Q \end{bmatrix}$$

$$\mathbf{M}_u = \bar{q}S \begin{bmatrix} bC_{l\delta_a} & 0 & bC_{l\delta_r} \\ 0 & \bar{c}C_{m\delta_e} & 0 \\ bC_{n\delta_a} & 0 & bC_{n\delta_r} \end{bmatrix} + \bar{q}_{\boldsymbol{prop}}S \begin{bmatrix} dC_{l\delta_a} & 0 & dC_{l\delta_r} \\ 0 & \bar{c}C_{m\delta_e} & 0 \\ dC_{n\delta_a} & 0 & dC_{n\delta_r} \end{bmatrix}$$

$$\mathbf{C}^{B/I} = \begin{bmatrix} {q_1}^2\text{-}{q_2}^2\text{-}{q_3}^2\text{+}{q_4}^2 & 2(q_1q_2\text{+}q_3q_4) & 2(q_1q_3\text{-}q_2q_4) \\ 2(q_1q_2\text{-}q_3q_4) & {q_2}^2\text{-}{q_3}^2\text{-}{q_1}^2\text{+}{q_4}^2 & 2(q_2q_3\text{-}q_1q_4) \\ 2(q_1q_3\text{+}q_2q_4) & 2(q_2q_3\text{-}q_1q_4) & {q_3}^2\text{-}{q_1}^2\text{-}{q_2}^2\text{+}{q_4}^2 \end{bmatrix}$$

α and β denote angle of attack and sideslip angle. $\mathbf{g}$ is the gravitational acceleration and m is the mass of UAV. b, $\bar{c}$, S, d, and $\mathbf{J}$ are the span of main plane, the mean aerodynamic chord, the wing area, the diameter of propeller, and the inertia tensor, respectively. The physical quantities regarding propeller are denoted by the subscript "*prop*". $\bar{q}$ is the dynamic pressure that generated by motion of UAV. $\bar{q}_{prop}$ is the dynamic pressure generated by the propeller slipstream. Aerodynamic coefficients in terms of the angle of attack are expressed by such as $C_L(\alpha)$, $C_D(\alpha)$, and $C_m(\alpha)$. $\mathbf{C}^{B/I}$ denotes the transformation matrix from an inertial coordinate system to body-fixed coordinate system using quaternion.

III. Flight Control System[7][8]

The proposed flight control system consists of translational and rotational controllers. Dynamic inversion method is applied to both controllers to linearize the dynamics of a UAV. Fig.2 shows a block diagram of the proposed flight control system.

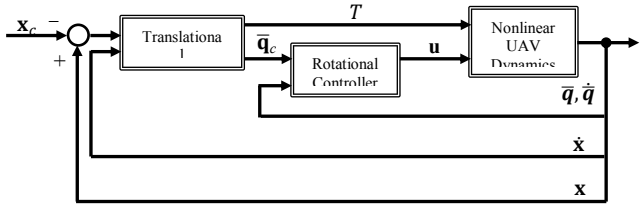

Fig. 2. Block diagram of flight control system.

A. Translational controller

A position error $\mathbf{x}_e$ is obtained from the difference in a current position $\mathbf{x}$ and desired position $\mathbf{x}_c$.

$$\mathbf{x}_e = \mathbf{x} - \mathbf{x}_c = [x - x_c \quad y - y_c \quad z - z_c]^T \quad (3)$$

The acceleration of UAV as shown in the following equation using the transform matrix $\mathbf{C}^{I/B}$ and velocity vector $\mathbf{V}$.

$$\ddot{\mathbf{x}}_e = \dot{\mathbf{C}}^{I/B}\mathbf{V} + \mathbf{C}^{I/B}\dot{\mathbf{V}} \quad (4)$$

Substituting this formula into the translational motion (1), the following equation is obtained.

$$\ddot{\mathbf{x}}_e = \dot{\mathbf{C}}^{I/B}\mathbf{V} - \mathbf{C}^{I/B}\tilde{\boldsymbol{\omega}}\mathbf{V} - \mathbf{g} - \tfrac{1}{\mathrm{m}}\mathbf{C}^{I/B}\mathbf{C}(\alpha)\mathbf{F} + \tfrac{1}{\mathrm{m}}\mathbf{T}^{I/B} = \mathbf{z}_{t1} + \mathbf{g}_t\mathbf{T}^{I/B} \quad (5)$$

Here $\mathbf{T}^{I/B}$, which is represented as $\mathbf{T}^{I/B} = \mathbf{C}^{I/B}\mathbf{T} = [T_x \quad T_y \quad T_z]^{\mathrm{T}}$, is the thrust vector in the inertial coordinate system. $\mathbf{z}_{t1}$ is an nonlinear term that includes aerodynamic force $\mathbf{F}$. $\mathbf{z}_{t1}$ is estimated by an observer that is based on disturbance accommodating control (DAC) method. When designing the DAC observer, $\mathbf{z}_{t1}$ is defined as a polynomial of time *t*.

$$\mathbf{z}_{t1} = \mathbf{c}_{t1}\mathbf{t} + \mathbf{c}_{t0}, \quad \mathbf{z}_{t2} = \dot{\mathbf{z}}_{t1} = \mathbf{c}_{t1}, \quad \mathbf{z}_{t3} = \dot{\mathbf{z}}_{t2} = 0 \quad (6)$$

Equation (5) is rewritten using an estimated value by the DAC observer.

$$\ddot{\hat{\mathbf{x}}}_e = \hat{\mathbf{z}}_{t1} + \mathbf{g}_t\mathbf{T}^{I/B} + \mathbf{L}_t\left(\dot{\mathbf{x}}_e - \dot{\hat{\mathbf{x}}}_e\right) \quad (7)$$

where "^" denotes an estimated value, and $\mathbf{L}_t$ is an observer gain. The following equation is derived from the polynomial (6) and the observer (7).

$$\frac{d}{dt}\begin{bmatrix} \dot{\hat{\mathbf{x}}}_e \\ \hat{\mathbf{z}}_{t1} \\ \hat{\mathbf{z}}_{t2} \end{bmatrix} = \begin{bmatrix} \mathbf{0}_{3\times3} & \mathbf{I}_{3\times3} & \mathbf{0}_{3\times3} \\ \mathbf{0}_{3\times3} & \mathbf{0}_{3\times3} & \mathbf{I}_{3\times3} \\ \mathbf{0}_{3\times3} & \mathbf{0}_{3\times3} & \mathbf{0}_{3\times3} \end{bmatrix} + \begin{bmatrix} \mathbf{I}_{3\times3} \\ \mathbf{0}_{3\times3} \\ \mathbf{0}_{3\times3} \end{bmatrix}\mathbf{g}_t\mathbf{T}^{I/B} + \begin{bmatrix} \mathbf{L}_{t1} \\ \mathbf{L}_{t2} \\ \mathbf{L}_{t3} \end{bmatrix}\left(\dot{\mathbf{x}}_e - \dot{\hat{\mathbf{x}}}_e\right) \quad (8)$$

If estimated values converge immediately to actual values, the thrust $\mathbf{T}^{I/B}$ can be obtained as follows:

$$\mathbf{T}^{I/B} = \mathbf{g}_t{}^{-1}(-\hat{\mathbf{z}}_{t1} + \boldsymbol{\upsilon}_x) \quad (9)$$

$\boldsymbol{\upsilon}_x$ can be considered as a new control input for the linearized system (8). The new control input $\boldsymbol{\upsilon}_x$ is defined as a PD controller.

$$\boldsymbol{\upsilon}_x = \mathbf{k}_{t1}\mathbf{x}_e + \mathbf{k}_{t2}\dot{\mathbf{x}}_e \quad (10)$$

Here $\mathbf{k}_{t1}$ and $\mathbf{k}_{t1}$ are feedback gains. Thrust magnitude T is obtained in the following.

$$T = \sqrt{{T_x}^2 + {T_y}^2 + {T_z}^2} \quad (11)$$

Measured values from the sensors such as a GPS and an IMU include noise and errors. In addition, there exists a serious problem that accurate ground speed of UAV cannot be measured by the sensors. Therefore, we use the extended Kalman filter to estimate the current position $\mathbf{x}$ and its time derivative $\dot{\mathbf{x}}$. The state equation and observation equation are given in the following equation.

$$\mathbf{x}_{k+1} = \mathbf{F}\mathbf{x}_k + \mathbf{w}_k \tag{12}$$
$$\mathbf{y}_k = \mathbf{H}\mathbf{x}_k + \mathbf{v}_k \tag{13}$$

Here $\mathbf{w}_k$ and $\mathbf{v}_k$ are defined independent Gaussian white noise. $\mathbf{F}$, $\mathbf{H}$ and $\mathbf{x}_k$ are the system matrix, the observation matrix, and the state variable, respectively.

$$\mathbf{x}_k = [x(k), y(k), z(k), \dot{x}(k), \dot{y}(k), \dot{z}(k), \ddot{x}(k), \ddot{y}(k), \ddot{z}(k)]$$

$$\boldsymbol{F} = \begin{bmatrix} \mathbf{I}_{3\times3} & \Delta\boldsymbol{T}\times\mathbf{I}_{3\times3} & \frac{\Delta T^2}{2}\times\mathbf{I}_{3\times3} \\ \mathbf{0}_{3\times3} & \mathbf{I}_{3\times3} & \Delta\boldsymbol{T}\times\mathbf{I}_{3\times3} \\ \mathbf{0}_{3\times3} & \mathbf{0}_{3\times3} & \mathbf{I}_{3\times3} \end{bmatrix}, \boldsymbol{H} = \begin{bmatrix} \mathbf{I}_{3\times3} & \mathbf{0}_{3\times3} & \mathbf{0}_{3\times3} \\ \mathbf{0}_{3\times3} & \mathbf{0}_{3\times3} & \mathbf{0}_{3\times3} \\ \mathbf{0}_{3\times3} & \mathbf{0}_{3\times3} & \mathbf{I}_{3\times3} \end{bmatrix}$$

Fig.3 shows a block diagram of the proposed translational controller.

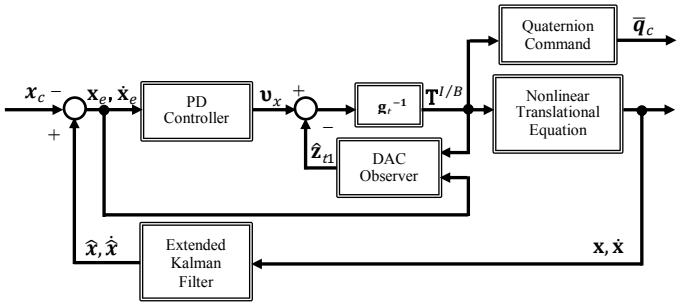

Fig. 3. Block diagram of translational controller.

B. Rotational controller

Commands for the rotational controller is generated by the thrust vector $\mathbf{T}^{I/B}$ because it is necessary to match the attitude of a UAV with the direction of thrust vector $\mathbf{T}^{I/B}$in the proposed control method. Commands of the pitch angle and heading angle are defined in the following equation.

$$\theta_c = \tan^{-1}(T_z/T_x), \Psi_c = \sin^{-1}(T_y/T) \tag{14}$$

Transforming each command angle (14) into quaternion to avoid a singular point, the following new commands are obtained.

$$\mathbf{q}_\theta = [0 \quad \sin(\theta_c/2) \quad 0 \quad \cos(\theta_c/2)]^T \tag{15}$$
$$\mathbf{q}_\psi = [0 \quad 0 \quad \sin(\Psi_c/2) \quad \cos(\Psi_c/2)]^T \tag{16}$$

The quaternion command is expressed by using (15) to (16).

$$\mathbf{q}_c = \begin{bmatrix} q_{c1} \\ q_{c2} \\ q_{c3} \\ q_{c4} \end{bmatrix} = \begin{bmatrix} q_{\theta4} & -q_{\theta3} & q_{\theta2} & q_{\theta1} \\ q_{\theta3} & q_{\theta4} & -q_{\theta1} & q_{\theta2} \\ -q_{\theta2} & q_{\theta1} & q_{\theta4} & q_{\theta3} \\ -q_{\theta1} & -q_{\theta2} & -q_{\theta3} & q_{\theta4} \end{bmatrix} \begin{bmatrix} q_{\psi1} \\ q_{\psi2} \\ q_{\psi3} \\ q_{\psi4} \end{bmatrix} \tag{17}$$

The rotational controller is designed in the similar procedure to translational controller. The kinematics relating to the quaternion is described using an angular velocity vector $\boldsymbol{\omega}$ and a skew-symmetric matrix $\bar{\mathbf{E}}(\mathbf{q})$.

$$\ddot{\bar{\mathbf{q}}} = \frac{1}{2}\dot{\bar{\mathbf{E}}}(\mathbf{q})\boldsymbol{\omega} + \frac{1}{2}\bar{\mathbf{E}}(\mathbf{q})\dot{\boldsymbol{\omega}} \tag{18}$$
$$\bar{\mathbf{E}}(\mathbf{q}) = \begin{bmatrix} q_4 & -q_3 & q_2 \\ q_3 & q_4 & -q_1 \\ -q_2 & q_1 & q_4 \end{bmatrix}$$

Substituting this formula into the rotational motion (2), the motion can be expressed by using the quaternion.

$$\ddot{\bar{\mathbf{q}}} = \frac{1}{2}\left\{\dot{\bar{\mathbf{E}}}(\mathbf{q})\boldsymbol{\omega} - \bar{\mathbf{E}}(\mathbf{q})\mathbf{J}^{-1}\widetilde{\boldsymbol{\omega}}\mathbf{J}\boldsymbol{\omega} + \bar{\mathbf{E}}(\mathbf{q})\mathbf{J}^{-1}\mathbf{M}\right\} + \frac{1}{2}\bar{\mathbf{E}}(\mathbf{q})\mathbf{J}^{-1}\mathbf{M}_u\mathbf{u} = \mathbf{z}_{r1} + \mathbf{g}_r\mathbf{u} \tag{19}$$

The nonlinear term $\mathbf{z}_{r1}$ is assumed as a polynomial of time t.

$$\mathbf{z}_{r1} = \mathbf{c}_{r1}\mathbf{t} + \mathbf{c}_{r0}$$
$$\mathbf{z}_{r2} = \dot{\mathbf{z}}_{r1} = \mathbf{c}_{r1}, \quad \mathbf{z}_{r3} = \dot{\mathbf{z}}_{r2} = 0 \tag{20}$$

Equation (19) is rewritten using an estimated value when we treat the DAC observer.

$$\ddot{\hat{\mathbf{q}}}_e = \hat{\mathbf{z}}_{r1} + \mathbf{g}_{r1}\mathbf{T}^{I/B} + \mathbf{L}_r\left(\dot{\bar{\mathbf{q}}}_e - \dot{\hat{\mathbf{q}}}_e\right) \tag{21}$$

The control input $\mathbf{u}$, which is to linearize the nonlinear equation (19), can be derived as follows:

$$\mathbf{u} = \mathbf{g}_r{}^{-1}\left(-\hat{\mathbf{z}}_{r1} + \boldsymbol{\upsilon}_q\right) \tag{22}$$

Here $\boldsymbol{\upsilon}_q$ is a new control input for the linearized system (23).

$$\frac{d}{dt}\begin{bmatrix} \bar{\mathbf{q}}_e \\ \dot{\bar{\mathbf{q}}}_e \end{bmatrix} = \begin{bmatrix} \mathbf{0}_{3\times3} & \mathbf{I}_{3\times3} \\ \mathbf{0}_{3\times3} & \mathbf{0}_{3\times3} \end{bmatrix}\begin{bmatrix} \bar{\mathbf{q}}_e \\ \dot{\bar{\mathbf{q}}}_e \end{bmatrix} + \begin{bmatrix} \mathbf{0}_{3\times3} \\ \mathbf{I}_{3\times3} \end{bmatrix}\boldsymbol{\upsilon}_q \tag{23}$$

The control input $\boldsymbol{\upsilon}_q$ is defined as the following equation. The H_∞control method is employed to decide the feedback gain $K(s)$.

$$\boldsymbol{\upsilon}_q = K(s)\begin{bmatrix} \bar{\mathbf{q}}_e \\ \dot{\bar{\mathbf{q}}}_e \end{bmatrix} \tag{24}$$

If the estimation error of the DAC observer is not sufficiently small, the nonlinear term is not completely canceled when using the dynamic inversion method. Then the error $\boldsymbol{\Delta}$ is treated as an uncertainty.

$$\ddot{\bar{\mathbf{q}}} = \mathbf{z}_{r1} + \mathbf{g}_r\mathbf{g}_r^{-1}\left(-\hat{\mathbf{z}}_{r1} + \boldsymbol{\upsilon}_q\right) = (\mathbf{z}_{r1} - \hat{\mathbf{z}}_{r1}) + \boldsymbol{\upsilon}_q = \boldsymbol{\Delta} + \boldsymbol{\upsilon}_q \tag{25}$$

$$\frac{d}{dt}\begin{bmatrix} \bar{\mathbf{q}}_e \\ \dot{\bar{\mathbf{q}}}_e \end{bmatrix} = \begin{bmatrix} \mathbf{0}_{3\times3} & \mathbf{I}_{3\times3} \\ \mathbf{0}_{3\times3} & \mathbf{0}_{3\times3} \end{bmatrix}\begin{bmatrix} \bar{\mathbf{q}}_e \\ \dot{\bar{\mathbf{q}}}_e \end{bmatrix} + \begin{bmatrix} \mathbf{0}_{3\times3} \\ \mathbf{I}_{3\times3} \end{bmatrix}\boldsymbol{\upsilon}_q + \begin{bmatrix} \mathbf{0}_{3\times3} \\ \mathbf{I}_{3\times3} \end{bmatrix}\boldsymbol{\Delta} \tag{26}$$

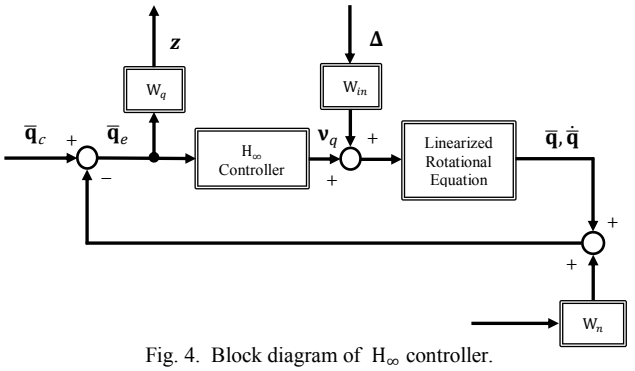

Fig. 4. Block diagram of H_∞ controller.

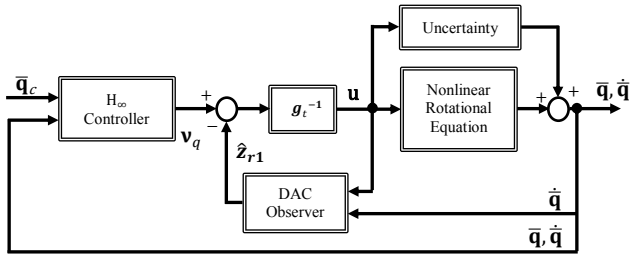

Fig. 5. Block diagram of rotational controller.

It is clear from the error quaternion (26) that each quaternion can be rewritten as the following equations.

$$\frac{d}{dt}\begin{bmatrix}\bar{\mathrm{q}}_{ei}\\ \dot{\bar{\mathrm{q}}}_{ei}\end{bmatrix}=\begin{bmatrix}0 & 1\\ 0 & 0\end{bmatrix}\begin{bmatrix}\bar{\mathrm{q}}_{ei}\\ i\end{bmatrix}+\begin{bmatrix}0\\ 1\end{bmatrix}\upsilon_{qi}+\begin{bmatrix}0\\ 1\end{bmatrix}\Delta,\ i=1,2,3 \qquad (27)$$

The H_∞ controller is designed to suppress not only the influence of the uncertainty but also disturbances such as gust of wind. The block diagram of the H_∞ controller and the rotational controller are shown in Figs.4 and 5. W_{in} as shown in Fig.4 denotes weighting function for a multiplicative uncertainty. W_n and W_q are weighting functions for sensor noise and the error between the quaternion command $\mathbf{q}_c$ and the current quaternion $\mathbf{q}$, respectively.

IV. Numerical simulation

A wind disturbance, which is expressed by using Dryden model, is applied to the dynamical model of a UAV. The mean speed of the wind is set to be 2.5 (m/s). The moment of inertia and the product of inertia in the inertial tensor are identified experimentally. We compare the flight control system using a PD controller for the rotational motion with the proposed flight control system. Tables I and II show initial conditions and constraints on control inputs in this numerical simulation, respectively. Results of numerical simulations are shown in Figs.6 to 8.

The UAV using the PD controller for the rotational motion cannot reach the desired position due to the influence of the wind disturbance. On the other hand, the UAV using the control system reached the desired point within about 20 seconds. It is clear from Figs.7(b) and 8(b) that the quaternions of the proposed system converge to constant values in comparison with quaternions of the system using PD controller. The control input of the proposed system did not exceed those limits shown in Table II. These indicate that the H_∞ controller is useful for the suppression of the wind disturbance in this case.

V. Experiments

We perform an experiment to verify the validity of the proposed flight control system. In Also in this experiment, we compare the flight control system using a PD controller with the controller in the same manner as the numerical simulation.

The overview and the specification of the developed UAV are shown in Fig.9 and Table III. GPS, IMU, microcomputer, and a radio module are equipped in the UAV. The radio module is used to transmit state variables and control inputs to the ground station. The desired position was set to $\mathbf{x}_c = [30 \quad 0 \quad -30]^T$(m). The wind speed was about 4 (m/s).

It can be seen from Figs.11(a) and (b) that the UAV arrives around the desired position although the attitude become unstable over time. It is shown from Fig.11(c) that control inputs exceed those constraints on the developed UAV. The thrust never exceed its upper bound during the control of the UAV. Control inputs were saturated as shown in Figs.12(c) and (d) when using the PD controller for the rotational motion. The controller was not able to reach the desired position and to keep attitude as shown in Figs.12(a) and (b).

VI. Conclusion

In this study, we proposed the flight control system using the dynamic inversion method. The design concept is no switching controller and dynamics of a fixed-wing UAV during transition flight to guarantee the stability of the system. The H_∞ controller was treated to suppress the wind disturbances. Numerical and experimental results showed the validity of the proposed flight control system.

References

[1] K. Muraoka, N. Okada, and D. Kubo, "Quad Tilt Wing VTOL UAV: Aerodynamic Characteristics and Prototype Flight Test," AIAA, Unmanned…Unlimited Conference, 2009, AIAA-2009-1834.

[2] J. H. Lee, B. M. Min, and E. T. Kim, "Autopilot Design of Tilt-rotor UAV Using Particle Swarm Optimization Method, International Conference on Control," Automation and Systems, 2007, pp.1629-1633.

[3] V. Myrand-Lapierre, A. Desbiens, E. Gagnon, F. Wong, and E. Poulin, "Transitions Between Level Flight and Hovering for a Fixed-Wing Mini Aerial Vehicle," Proceedings of the American Control Conference, 2010, pp.530-535.

[4] Y. Akai, Y. Shimada, K. Uchiyama, and A. Abe,."Design of Nonlinear Attitude Control System for Spaceplane Using Disturbance-Accommodating Control," Proceedings of KSAS-JSASS Joint International Symposium on Aerospace Engineering, 2008, pp.542-547.

[5] C. D. Johnson, "A Family of "Universal Adaptive Controllers" for Linear and Nonlinear Plants," Proceedings of the Twentieth Southeastern Symposium on System Theory, 1988, pp.530-534.

[6] R. Giroux, R. Gourdeau, and R. Landry, "Extended Kalman Filter Implementation for Lo-cost INS/GPS Integration in a Fast Prototyping Environment," 16th Symposium on Navigation of the Canadian Navigation society, 2005, pp.1-11.

[7] M. Kokume and K. Uchiyama, "Control Architecture for Transition between Level Flight to Hovering of a Fixed-Wing UAV," Journal of JSASS, Vol.60, 2012, pp173-180. (in Japanese)

[8] K. Iwasaki and K. Uchiyama "Robust Controller Design for Transition Flight for Fixed-Wing UAV," Proceedings of Asia-Pacific International Symposium on Aerospace Technology (APISAT), 2012, CD-ROM 7.5.2.

Table I. Initial conditions

Attitude angles $\mathbf{q}_0$ [-]	$[0 \quad 0 \quad 0 \quad 1]^T$
Velocities $\mathbf{V}_0$ [m/s]	$[13.5 \quad 0 \quad 0]^T$
Angular rates $\boldsymbol{\omega}_0$ [rad/s]	$[0 \quad 0 \quad 0]^T$
Positions $\mathbf{x}_0$ [m]	$[0 \quad 0 \quad 0]^T$
Desired positions $\mathbf{x}_c$ [m]	$[60 \quad 30 \quad -60]^T$

Table II. Constraints on control input

Aileron angles δ_a [deg]	± 32
Rudder angles δ_e [deg]	± 54
Elevator angles δ_r [deg]	± 58
Thrust T [N]	9

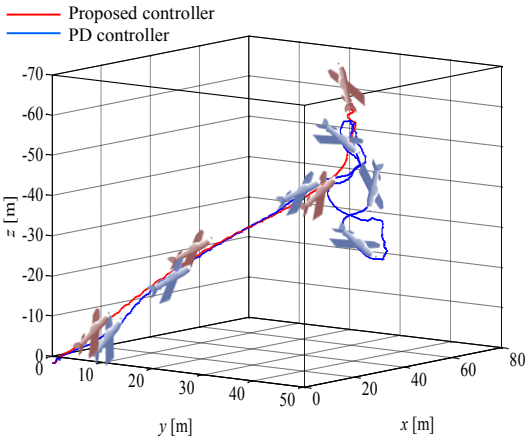

Fig. 6. Trajectories of UAV.

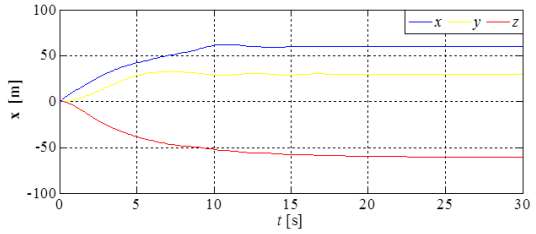

(a) Position

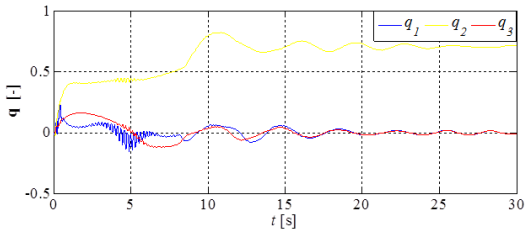

(b) Quaternion

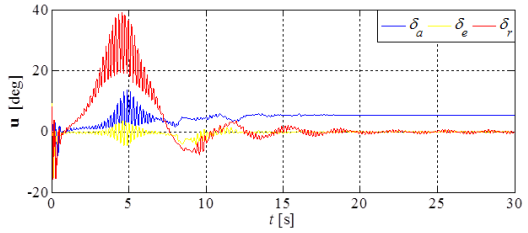

(c) Moving surfaces

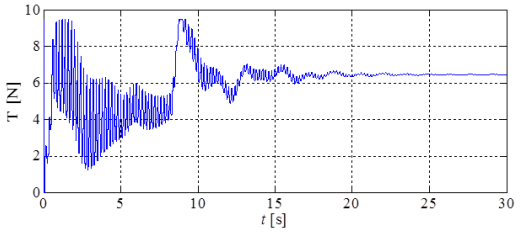

(d) Thrust

Fig. 7. Time response of UAV using proposed controller (H_∞ controller).

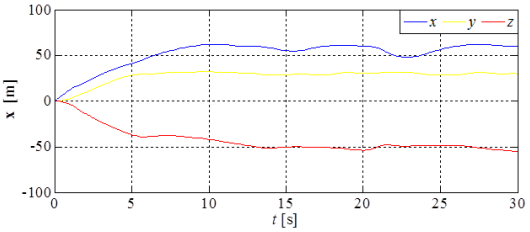

(a) Position

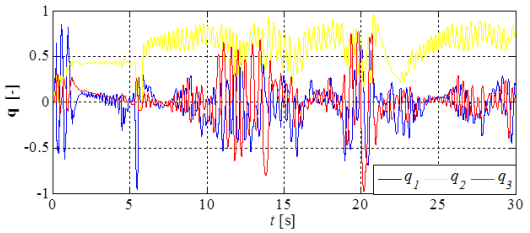

(b) Quaternion

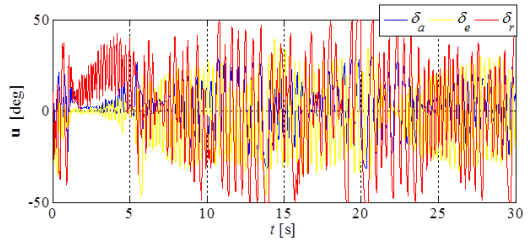

(c) Moving surfaces

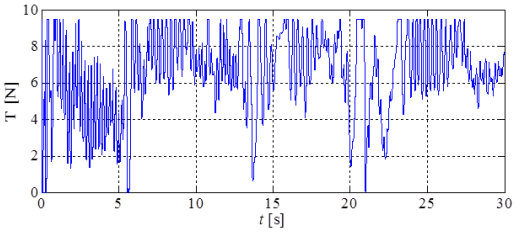

(d) Thrust

Fig. 8. Time response of UAV using PD controller.

Fig. 9. Overview of developed UAV.

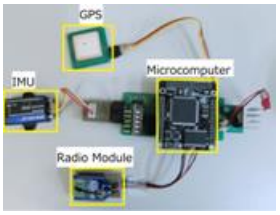

Fig. 10. Avionics of UAV.

Table III. Specification of UAV

Wing span [mm]	900
Length [mm]	1020
Mass [kg]	0.66
Material	EPP

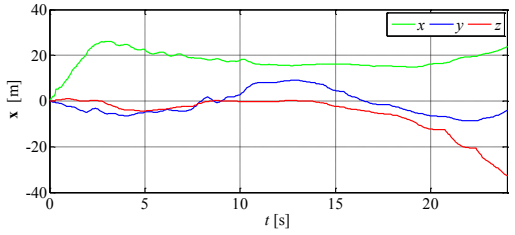

(a) Position

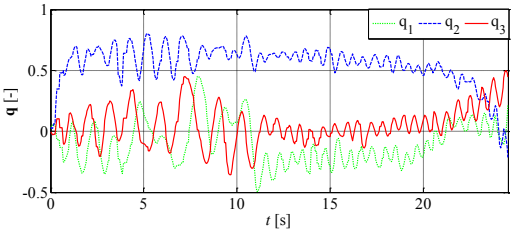

(b) Quaternion

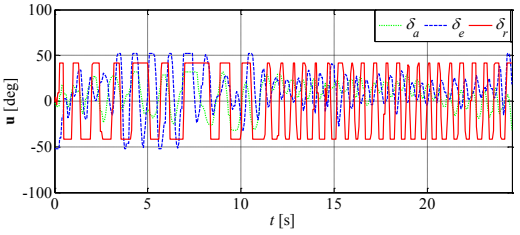

(c) Moving surfaces

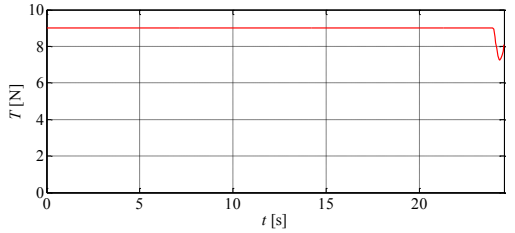

(d) Thrust

Fig. 11. Experimental results of UAV using proposed controller (H_∞ controller).

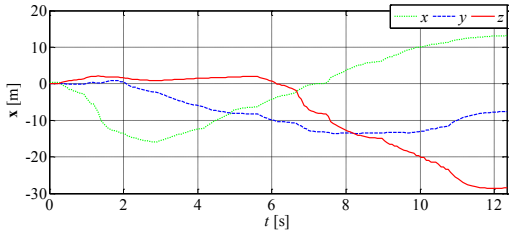

(a) Position

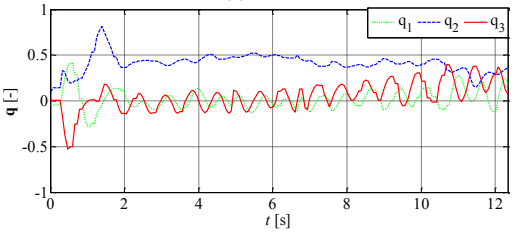

(b) Quaternion

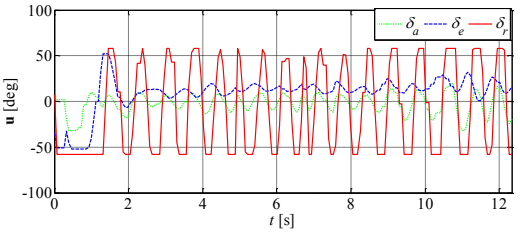

(c) Moving surfaces

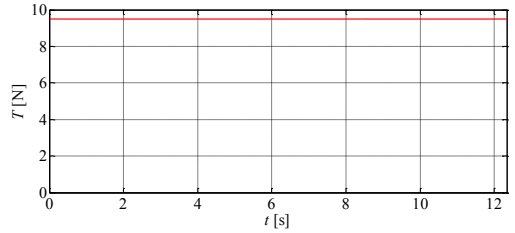

(d) Thrust

Fig. 12. Experimental results of UAV using PD controller.